

# Robust Online Multi-target Visual Tracking using a HISP Filter with Discriminative Deep Appearance Learning

Nathanael L. Baisa\*, *Member, IEEE*,

**Abstract**—We propose a novel online multi-target visual tracker based on the recently developed Hypothesized and Independent Stochastic Population (HISP) filter. The HISP filter combines advantages of traditional tracking approaches like multiple hypothesis tracking (MHT) and point-process-based approaches like probability hypothesis density (PHD) filter, and has a linear complexity while maintaining track identities. We apply this filter for tracking multiple targets in video sequences acquired under varying environmental conditions and targets density using a tracking-by-detection approach. We also adopt deep convolutional neural networks (CNN) appearance representation by training a verification-identification network (VerIdNet) on large-scale person re-identification data sets. We construct an augmented likelihood in a principled manner using this deep CNN appearance features and spatio-temporal (motion) information that can improve the tracker's performance. In addition, we solve the problem of two or more targets having identical label taking into account the weight propagated with each confirmed hypothesis. Finally, we carry out extensive experiments on Multiple Object Tracking 2016 (MOT16) and 2017 (MOT17) benchmark data sets and find out that our tracker significantly outperforms several state-of-the-art trackers in terms of tracking accuracy.

**Index Terms**—Visual tracking, Multiple target filtering, HISP filter, MHT, PHD filter, MOT Challenge.

## I. INTRODUCTION

Multi-target tracking is an active research field in computer vision with a wide variety of applications such as intelligent surveillance, autonomous driving, robot navigation and augmented reality. It essentially associates the estimated states (from noisy observations) corresponding to the same object over time i.e. it assigns consistent labels to the tracked targets in each video frame to generate a trajectory for each target. These can be performed using online tracking based on Bayesian filtering [1] [2] [3] or offline tracking based on global optimization-based data association [4] [5] [6]. Online methods estimate the target state at each time instant and depends on predictive models in case of miss-detections to carry on tracking, however, both past and future observations are used in offline (batch) methods to overcome miss-detections. Although offline trackers can generally outperform the online trackers, they are limited for time-critical real-time applications such as autonomous driving and robot navigation where it is crucial to deliver estimates as observations arrive.

A multi-target tracker receives a random number of measurements from a target detection process applied to the source data such as video frames. Thus, the multi-target tracker has to deal with measurement origin uncertainty, false alarms, missed detections, and the births and deaths of targets in addition to process and measurement noises. Comprehensive surveys of multi-target tracking methods can be found in [7] [8]. In particular, three data association algorithms, Global Nearest Neighbor (GNN) [9], Joint Probabilistic Data Association Filter (JPDAF) [9] and Multiple Hypothesis Tracking (MHT) [9], [10], have been widely used for more than three decades. All of these methods have significant complexity, although the performance and computational cost of the MHT is much higher than that of the GNN or JPDAF. In part due to the complexity of these approaches, random finite set (RFS) multi-target tracking algorithms [11] have received a great deal of attention. This paradigm includes all sources of uncertainty in a unified framework. The probability hypothesis density (PHD) filter [12] is the most widely adopted RFS-based filter for visual tracking in computer vision. However, this filter does not include target identity in the framework. Recently, a new filter, Hypothesized and Independent Stochastic Population (HISP) filter [13]–[15], based on the stochastic populations has been proposed which includes all sources of uncertainty in a unified framework with a linear complexity while maintaining track identities.

More recently, Convolutional Neural Network (CNN) features have demonstrated outstanding results on various recognition tasks [16] [17]. They have also shown better performance on object detection [18] and person re-identification [19] problems. Motivated by this, some deep learning based trackers have been developed [4], [20] due to their powerful capturing capability of discriminative appearance features of a target of interest against background and other similar objects. However, the advantages of CNNs in stochastic population based filters, such as HISP filter, have not been explored which works online and suitable for real-time applications.

In this work, we propose an online multi-target visual tracker which jointly addresses track management (target birth, death and labeling), miss-detection and clutter within a single Bayesian framework using a tracking-by-detection approach for time-critical real-time applications. Our proposed tracker is based on the recently developed HISP filter. We also learn discriminative deep appearance features of targets using a Verification-Identification CNN architecture (VerIdNet). We

\*N. L. Baisa is currently a research scientist at AnyVision. This work was done when the author was with the Department of Computer Science, University of Lincoln, Lincoln LN6 7TS, United Kingdom. (e-mail: NBaisa@lincoln.ac.uk).

construct a single augmented likelihood using this learned deep CNN appearance features and spatio-temporal (motion) information that can fit into the HISP filter for improving the tracker's performance. We also solve the problem of two or more targets having identical label that occurs using the track extraction method in the HISP filter taking into account the weight propagated with each confirmed hypothesis. To the best of our knowledge, nobody has adopted this approach using this new HISP Filter.

The main contributions of this paper are as follows:

- 1) We apply the HISP filter for tracking multiple targets in video sequences acquired under varying environmental conditions and targets density.
- 2) We construct an augmented likelihood using deeply learned CNN appearance features and motion information and then incorporate into the HISP filter.
- 3) We solve the problem of two or more targets having identical label taking into account the weight propagated with each confirmed hypothesis.
- 4) We make extensive experiments on Multiple Object Tracking 2016 (MOT16) and MOT17 benchmark data sets using the public detections provided in the benchmark's test sets.

We presented a preliminary idea of this work in [21]. In this work, we make more elaborate descriptions of our algorithm. Besides, we include deep CNN appearance features in addition to motion information to construct a single augmented likelihood that can fit into the HISP filter. We also make extensive evaluations on MOT17 in addition to MOT16 benchmark data set.

The rest of this paper is organized as follows. After the discussion of related work in section II, the HISP filter in video tracking context is described in detail including the modelling of the augmented likelihood in section III. The discriminative deep appearance learning using VerIdNet is explained in section IV, and section V provides the applications and determination of some important variable values in the HISP filter. The experimental results are analyzed and compared in section VI followed by the summary of the main conclusions and suggestions for future work in section VII.

## II. RELATED WORK

Traditionally, multi-target trackers have been developed by finding associations between targets and observations using JPDAF [9] and MHT [9], [10]. However, these approaches have faced challenges not only in the uncertainty caused by data association but also in algorithmic complexity that increases exponentially with the number of targets and measurements. Recently, a unified framework which directly extends single to multiple target tracking by representing multi-target states and observations as RFS was developed by Mahler [12] which not only addresses the problem of increasing complexity, but also estimates the states and cardinality of an unknown and time varying number of targets in the scene by allowing for target birth, death, clutter (false alarms), and missing detections. It propagates the first-order moment of the multi-target posterior, called the PHD [22], rather than the full

multi-target posterior. This approach is flexible, for instance, it has been used to find the detection proposal with the maximum weight as the target position estimate for tracking a target of interest in sparse as well as in dense environments by removing the other detection proposals as clutter [23] [24]. Furthermore, the standard PHD filter was extended to develop a novel N-type PHD filter ( $N \geq 2$ ) for tracking multiple target of different types in the same scene [25] [26]. However, this approach does not include target identity in the framework because of the indistinguishability assumption of the point process; additional mechanism is necessary for labeling each target either at the prediction stage [1] or by post-processing the filter outputs [26]. Recently, labeled RFS for multi-target tracking was introduced in [27] [28] [29], however, its computational complexity is high. In general, the RFS-based filters are susceptible to miss-detection even though they are robust to clutter.

More recently, the estimation framework for stochastic populations has been put forward which proposes a probabilistic representation of the population of interest through two levels of uncertainty: on the individual and population levels i.e. the targets of the population of interest are represented by tracks and the composition of the population of interest is represented by multi-target configurations. A new filter based on this stochastic populations has been developed with the concept of partially-distinguishable populations and is termed as Distinguishable and Independent Stochastic Populations (DISP) filter [30]. This filter can handle an unknown and time varying number of targets in the scene with targets birth, death, miss-detections and false alarms, however, it has a high computational complexity. A low-complexity filter called HISP filter [13] has been derived from the DISP filter under some intuitive approximations and was adapted for space situational awareness in [14], [15]. This HISP filter has a linear complexity with both the number of hypotheses and the number of observations similar to the PHD filter, however, unlike the PHD filter, it can preserve the distinct tracks for detected targets.

Appearance information has been included in some works such as [3], [10], [29], [31]. Appearance models of targets are learned in an online fashion via a multi-output regularized least squares (MORLS) framework and are incorporated into the tree-based track-oriented MHT (TO-MHT) in [10], however, the tracker works offline and is computationally expensive. Similar approach has been employed in [29] to learn the appearance models of targets and then to include this appearance information into a generalized labeled multi-Bernoulli (GLMB) filter. Though this GLMB-based tracker operates online, it is computationally expensive. Deep appearance features have also been incorporated into the PHD filter in [3], [31], however, the PHD filter is generally vulnerable to miss-detection though computationally efficient and robust to clutter. To date, no work has incorporated appearance information into the recently proposed stochastic populations based filters and applied for visual tracking, as is the case in our work.

### III. THE HISP FILTER

The HISP filter is a principled approximation of the DISP filter for practical applications especially for filtering in scenarios involving a large number of targets with moderately ambiguous data association. It combines the advantages of engineering solutions like MHT and point-process-based approaches like PHD filter. It propagates track identities through time similar to MHT, however, it overcomes the drawbacks of MHT such as its strong reliance on heuristics for the appearance and disappearance of targets and a lack of adaptivity, by modelling all sources of uncertainties in a unified probabilistic framework. Moreover, it has a linear complexity in the number of hypotheses and in the number of observations, however, the MHT filter has an exponential complexity with time.

Let the time be indexed by the set  $\mathbb{T} \doteq \mathbb{N}$ . For any  $t \in \mathbb{T}$ , the target state space of interest and the observation space of interest are given by  $\mathbf{X}_t^\bullet \subseteq \mathbb{R}^d$  and  $\mathbf{Z}_t^\bullet \subseteq \mathbb{R}^{d'}$ , respectively, with the integers  $d$  and  $d'$  usually verifying  $d \geq d'$ . They are augmented with the empty state  $\psi_{es}$  and false-alarm generators  $\psi_{fa}$  which describe the state of targets not in the area of interest and the objects in the field of view of the sensor that are not of direct interest but which may interfere with the observation of the targets, respectively, and the empty observation  $\phi$  which describes missed detections, to form the (full) target state space  $\mathbf{X}_t = \mathbf{X}_t^\bullet \cup \{\psi_{es}, \psi_{fa}\}$  and the (full) observation space  $\mathbf{Z}_t = \mathbf{Z}_t^\bullet \cup \{\phi\}$ . The set of collected observations is represented by  $\bar{Z}_t = Z_t \cup \{\phi\}$ ;  $Z_t$  for detected observations.

At any time  $t \in \mathbb{T}$ , the HISP filter is basically based on the following modelling assumptions: 1) a target produces at most one observation (if not, a miss detection occurs), 2) an observation originates from at most one target (if not, a false alarm occurs), 3) targets evolve independently of each other, and 4) observations resulting from target detections are produced independently from each other.

For tracking applications, targets are distinguished by considering their observation histories. Let the space  $\mathbb{O}_t$  be defined as the Cartesian product

$$\bar{\mathbb{O}}_t = \bar{Z}_0 \times \dots \times \bar{Z}_t, \quad (1)$$

so that  $\mathbf{o}_t \in \mathbb{O}_t$  takes the form  $\mathbf{o}_t = (\phi, \dots, \phi, z_{t_+}, \dots, z_{t_-}, \phi, \dots, \phi)$  with  $t_+$  and  $t_-$  the time of appearance and disappearance of the considered track in the scene of interest, and with  $z_t \in \bar{Z}_t$  for any  $t_+ \leq t \leq t_-$ . The observation history  $\mathbf{o}_t$  can also be referred to as the observation path and the empty observation path  $(\phi, \dots, \phi) \in \mathbb{O}_t$  is denoted by  $\phi_t$ .

Each target is identified by some index  $i$  in a set  $\mathbb{I}$ . An observation characterizes an individual target. A track  $i$  associated to an observation path with at least one detection (i.e.  $\mathbf{o}_t^i \neq \phi_t$ ) cannot have a multiplicity  $n^i$  greater than one since it cannot represent more than one target, hence, the *previously-detected* target represented by the track  $i$  is then *distinguishable*. However, a track  $i$  associated to the empty observation path  $\mathbf{o}_t^i = \phi_t$  represents a sub-population of *yet-to-be-detected* (undetected) targets that are *indistinguishable* from one another, and may have a multiplicity  $n^i$  greater than

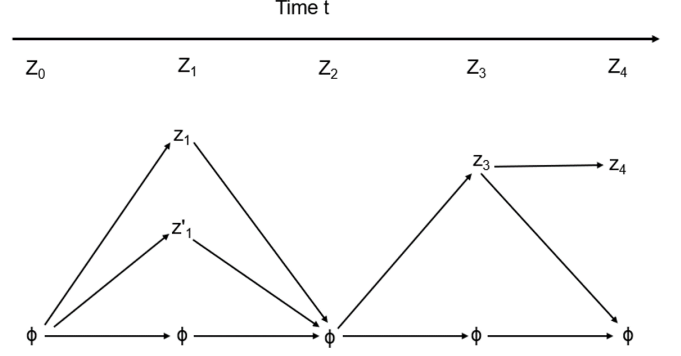


Fig. 1: The observation paths at time  $t = 4$  of the HISP filter.

one. The tracks cover all the possible combinations of non-empty observation paths representing the previously-detected targets, and one (or possibly several) track(s) representing sub-population(s) of yet-to-be-detected targets. For instance, the observation paths at time  $t = 4$ , given a sequence of collected observations, is shown in Fig. 1. This diagrammatic illustration is somehow similar to a non-tree based track-oriented MHT [8]. The observation paths in the diagram of Fig. 1 can be explicitly listed as:

$$\begin{aligned} (\phi, \phi, \phi, \phi, \phi) &= \phi & (2) \\ (\phi, \phi, \phi, z_3, \phi) \\ (\phi, \phi, \phi, z_3, z_4) \\ (\phi, z'_1, \phi, \phi, \phi) \\ (\phi, z'_1, \phi, z_3, \phi) \\ (\phi, z'_1, \phi, z_3, z_4) \\ (\phi, z_1, \phi, \phi, \phi) \\ (\phi, z_1, \phi, z_3, \phi) \\ (\phi, z_1, \phi, z_3, z_4) \end{aligned}$$

Each subset of pairwise compatible tracks  $H \subseteq \mathbb{I}_t \setminus \{u\}$  which represents the previously-detected targets is called an hypothesis, and the set of all the hypotheses is represented by  $\mathbf{H}_t$  whereas the undetected track  $u$ , with multiplicity  $n^u \in \mathbb{N}$ , denotes sub-populations of  $n^u$  yet-to-be-detected targets. Each element in the set  $\mathbb{I}_t^u$  is denoted by  $i_t^u$ . The HISP filter maintain a single track  $u \in \mathbb{I}$  for all the undetected targets. In the HISP filter, hypotheses are assumed to be independent of each other.

Accordingly, a target is indexed by a pair  $(t, \mathbf{o})$ , i.e.  $\mathbf{i} = (t, \mathbf{o})$ , where  $t$  is the last epoch where the target was known to be in the scene, and the observation path  $\mathbf{o}$  stores its detections across time. Thus, at any time  $t \in \mathbb{T}$ , the representation of targets after the prediction and after the update steps can be indexed by the sets  $\mathbb{I}_{t|t-1} = \{(t, \mathbf{o}) | \mathbf{o} \in \bar{\mathbb{O}}_{t-1}\}$  and  $\mathbb{I}_t = \{(t, \mathbf{o}) | \mathbf{o} \in \bar{\mathbb{O}}_t\}$ , respectively. The other important notation is an indicator function, for instance, on the set  $A$  can be expressed as

$$\mathbf{1}_A(x) = \begin{cases} 1, & \text{if } x \in A \\ 0, & \text{otherwise} \end{cases} \quad (3)$$

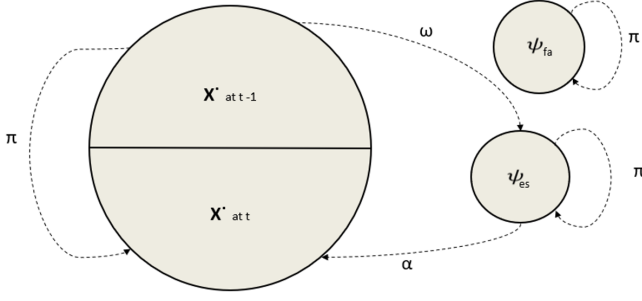


Fig. 2: The transition functions' relation between times  $t-1$  and  $t$  for the subsets of  $\mathbf{X}$ .

Using the aforementioned notations and concept, the HISP filter can be expressed via a set of hypotheses. For instance, after the observation (data) update step at time  $t$  (see section III-B), it can be expressed by set of triples (multi-target configuration) of the form  $\mathcal{P}_t = \{p_t^i, w_t^i, n_t^i\}_{i \in \mathbb{I}_t}$ , where  $p_t^i$  is the probability density corresponding to the index  $i \in \mathbb{I}_t$ ,  $w_t^i \in [0, 1]$  is the weight (or probability of existence) of the hypothesis, and  $n_t^i$  is the multiplicity of the hypothesis. Each hypothesis maintained by the HISP filter corresponds to a track (a confirmed hypothesis, see section III-D) and is described by its own probability of existence.

The important steps of the HISP filter are briefly described as follows.

#### A. Time Prediction

The three (sub-)transition functions used for modelling the motion as well as the appearance and disappearance of targets between times  $t-1$  and  $t$  are (also shown in Fig. 2):

- 1)  $q_t^\alpha$  models target's appearance (birth) i.e. transition from  $\psi_{es}$  to  $\mathbf{X}^\bullet$ .
- 2)  $q_t^\pi$  models target's dynamics i.e. transitions from  $\mathbf{X}^\bullet$  to  $\mathbf{X}^\bullet$  or from  $\psi_{es}$  or  $\psi_{fa}$  to themselves.
- 3)  $q_t^\omega$  models target's disappearance (death) i.e. transition from  $\mathbf{X}^\bullet$  to  $\psi_{es}$ .

These functions are considered as sub-transitions since  $q_t^\iota(\cdot|x)$ ,  $\iota \in \{\pi, \alpha, \omega\}$ , is not a probability distribution in general but is assumed to verify  $\int q_t^\iota(x'|x)dx' \leq 1$ . There is no possible transition between the subset  $\mathbf{X}_t^\bullet \cup \{\psi_{es}\}$  describing the targets and the point  $\psi_{fa}$  describing the false-alarm generators, thus, it holds that

$$q_t^\iota(x'|\psi_{fa}) = q_t^\iota(\psi_{fa}|x) = 0, \quad (4)$$

for any  $x, x' \neq \psi_{fa}$ .

Accordingly, the motion of a target from time  $t-1$  to time  $t$  is modelled by a Markov transition  $q_t^\pi$  verifying for any  $x' \in \mathbf{X}_{t-1}^\bullet$

$$q_t^\pi(\psi_{es}|\psi_{es}) = 1 \quad \text{and} \quad q_t^\pi(\psi_{es}|x') = 0, \quad (5)$$

The transition  $q_t^\pi$  models propagation in the scene only, excluding target appearance and disappearance into (out of) the scene. The probability that a target at point  $x$  at time  $t-1$  does not disappear is given by the function  $p_t^\pi(x) = \int q_t^\pi(x'|x)dx'$ .

The disappearance of a target between time  $t-1$  and time  $t$  is modelled separately by a transition  $q_t^\omega$  verifying for any  $x' \in \mathbf{X}_{t-1}^\bullet$

$$q_t^\omega(x'|x)dx = 0 \quad \text{and} \quad q_t^\omega(x|\psi_{es})dx = 0, \quad (6)$$

It is assumed that the transition  $q_t^\pi$  and  $q_t^\omega$  are complementary in the sense that  $q_t^\omega(\psi_{es}|x) + p_t^\pi(x) = 1$ , i.e. a target with state  $x$  in  $\mathbf{X}^\bullet$  can either propagate to  $\mathbf{X}^\bullet$  with probability  $p_t^\pi(x) = \int q_t^\pi(x'|x)dx'$  or disappear and move to  $\psi_{es}$ . Hence, the probability of survival of target with state  $x$  is given by the scalar  $p_t^\pi(x) = 1 - q_t^\omega(\psi_{es}|x)$ . Besides, there are  $n_t^\alpha$  targets potentially appearing at time  $t$ , modelled by a probability density  $p_t^\alpha$  on  $\mathbf{X}_t$  and by a scalar  $w_t^\alpha$ .

In the estimation framework for stochastic populations, the appearing targets and the yet-to-be detected (undetected) targets are mixed in a single sub-population. Using "u" in place of the indices  $i_{t-1}^u$  and  $i_{t-1}^u$  when there is no possible ambiguity, the newborn and the undetected targets are represented together after time prediction by

$$p_{t|t-1}^u(x) = \frac{n_{t-1}^u \int q_t^\pi(x|x')p_{t-1}^u(x')dx' + n_t^\alpha p_t^\alpha(x)}{n_{t-1}^u + n_t^\alpha}, \quad (7a)$$

$$(w_{t|t-1}^u, n_{t|t-1}^u) = \left( \frac{n_{t-1}^u w_{t-1}^u + n_t^\alpha w_t^\alpha}{n_{t-1}^u + n_t^\alpha}, n_{t-1}^u + n_t^\alpha \right), \quad (7b)$$

Where  $p_t^\alpha(x) = q_t^\alpha(x|\psi_{es})$  is the distribution of appearing targets. The targets that have already been observed at least once in the past and which have prior indices in  $\mathbb{I}_{t-1}$  of the form  $\kappa = (t-1, \mathbf{o})$ , with  $\mathbf{o} \neq \phi_{t-1}$ , can either be propagated (kernel  $q_t^\pi$ ), and they are characterized after time prediction by

$$\tilde{p}_{t|t-1}^i(x) = \int q_t^\pi(x|x')p_{t-1}^{\kappa}(x')dx', \quad (8a)$$

$$w_{t|t-1}^i = w_{t-1}^{\kappa} \int \int q_t^\pi(x|x')p_{t-1}^{\kappa}(x')dx'dx, \quad (8b)$$

$$n_{t|t-1}^i = 1, \quad (8c)$$

or disappear (kernel  $q_t^\omega$ ), and they are characterized after time prediction by

$$p_{t|t-1}^{\kappa}(x) = \int q_t^\omega(\psi_{es}|x')p_{t-1}^{\kappa}(x')dx', \quad (9a)$$

$$w_{t|t-1}^{\kappa} = w_{t-1}^{\kappa} \int q_t^\omega(\psi_{es}|x')p_{t-1}^{\kappa}(x')dx', \quad (9b)$$

$$n_{t|t-1}^{\kappa} = 1, \quad (9c)$$

with  $i = (t, \mathbf{o}) \in \mathbb{I}_{t|t-1}$  (the target is still in the scene at epoch  $t$ ) and  $\kappa = (t-1, \mathbf{o}) \in \mathbb{I}_{t-1}$  (the target has left the scene since last epoch  $t-1$ ). Note that the index in  $\mathbb{I}_{t|t-1}$  of the corresponding hypothesis of disappeared one remains equal to  $\kappa$ . The single-target laws of disappeared targets are not very informative, however, they can be useful in practice as the scalar  $\int q_t^\omega(\psi|x)p_{t-1}^{\kappa}(x)dx$  gives the credibility of the hypothesis that the target with index  $\kappa$  at time  $t-1$  disappeared between  $t-1$  and  $t$ . The hypotheses corresponding



to disappeared targets are not indexed in the set  $\mathbb{I}_{t|t-1}$  since they are not considered for the following observation update. Though they are ignored for the purpose of filtering, they need to be stored as they will be useful for track extraction (see section III-D).

The approximated multi-target configuration  $\mathcal{P}_{t|t-1}$  after prediction from time  $t-1$  to time  $t$  is then given by  $\mathcal{P}_{t|t-1} = \{p_{t|t-1}^i, w_{t|t-1}^i, n_{t|t-1}^i\}_{i \in \mathbb{I}_{t|t-1}}$ . The time prediction step applies independently to each hypothesis as seen in the prediction equations (7), (8) and (9) due to the modelling assumption on the independence of the targets making it have a linear complexity with respect to the number of hypotheses.

### B. Observation Update with Augmented Likelihood

The observation process at time  $t$  is modelled by a potential  $\ell_t(z|\cdot)$  on  $\mathbf{X}_t$  defined for any  $z \in \bar{Z}_t$  and verifying  $\ell_t(\phi|\psi_{es}) = 1$  as no observation can be generated from targets that are not present in the scene. For any  $x \in \mathbf{X}_t^\bullet$ , the potential  $\ell_t(z|\cdot)$  can be given by

$$\ell_t(z|x) = p_{d,t}(x)g_t(z|x), \quad z \in Z_t \quad \text{and} \quad \ell_t(\phi|x) = 1 - p_{d,t}(x), \quad (10)$$

where  $p_{d,t}$  is the probability of detection and the dimensionless potential  $g_t(z|\cdot)$  is the *augmented likelihood* of association with measurement  $z$ . In this case, let  $z = (z_d, z_w) \in \bar{Z}_t$  be an ordered pair of a detection vector  $z_d$  and an appearance feature vector  $z_w$  which is extracted from the detected object region i.e. a region enclosed by a detection vector  $z_d$ . Assuming a paired observation  $z \in \bar{Z}_t$  is an ordered pair conditionally independent observations, the augmented likelihood can be given by

$$g_t(z|x) = g_t(z_d|x)g_t(z_w|x), \quad (11)$$

where the appearance feature likelihood function  $g_t(z_w|x)$  will be discussed in Section IV-A. The detection vector likelihood is given in the two-dimensional, linear Gaussian case as

$$g_t(z_d|x) = \exp\left(-\frac{1}{2}(Hx - z_d)^T S^{-1}(Hx - z_d)\right), \quad (12)$$

where  $H$  is the observation matrix and  $S$  is the innovation covariance. With this approach, the probability for the observation  $z$  to belong to the target with distribution  $p$  is given by

$$\int g_t(z|x)p(x)dx = g_t(z_w|x)\sqrt{\frac{|R|}{|S|}}\exp\left(-\frac{1}{2}(Hx - z_d)^T S^{-1}(Hx - z_d)\right), \quad (13)$$

which is dimensionless and takes values in the interval  $[0, 1]$ , and  $|\cdot|$  is the determinant. The  $g_t(z_w|x)$  will be given in Section IV-A.

To maintain a low computational cost for the HISP filter, all the terms in the observation update can be computed with a linear complexity by making an assumption on the term

$$\tilde{w}_t^{\kappa,z} = w_{t|t-1}^{\kappa} \int \ell_t(z|x)p_{t|t-1}^{\kappa}(x)dx \quad (14)$$

which corresponds to the *association weight* of the target with index  $\kappa \in \mathbb{I}_{t|t-1}$  with the observation  $z \in Z_t$ .

For any  $\kappa = (t, \mathbf{o}) \in \mathbb{I}_{t|t-1}$  and any  $z \in \bar{Z}_t$ , define  $\mathbf{i}$  as the index  $(t, \mathbf{o} \times z)$ , with  $(\mathbf{o} \times z)$  being the concatenation of  $\mathbf{o}$  and  $z$ , and define  $p_t^i$  as the probability density function on  $\mathbf{X}_t$  characterized by

$$p_t^i(x) = \frac{\ell_t(z|x)p_{t|t-1}^{\kappa}(x)}{\int \ell_t(z|x')p_{t|t-1}^{\kappa}(x')dx'} \quad (15)$$

for any  $x \in \mathbf{X}_t$  and let the weights be characterized equivalently by

$$w_t^i = \frac{w_{ex}^{\kappa,z} \tilde{w}_t^{\kappa,z}}{\sum_{z' \in \bar{Z}_t} w_{ex}^{\kappa,z'} w_t^{\kappa,z'}} \quad \text{or} \quad w_t^i = \frac{w_{ex}^{\kappa,z} \tilde{w}_t^{\kappa,z}}{\sum_{\kappa' \in \mathbb{I}_{t|t-1}} w_{ex}^{\kappa',z} w_t^{\kappa',z}} \quad (16)$$

where the scalar  $w_t^{\kappa,z} = \tilde{w}_t^{\kappa,z} + \mathbf{1}_\phi(z)(1 - w_{t|t-1}^{\kappa})$  is the probability mass attributed to the association between  $\kappa$  and  $z$  including the possibility that the target does not actually exist in the case of detection failure. The probability that a false alarm will be generated for  $z \in \bar{Z}_t$  is denoted by  $v_t(z)$ . The posterior probability for an observation  $z \in Z_t$  to be a false alarm is also obtained via (16) when  $\kappa = z$ , by setting  $w_t^{z,z} = \tilde{w}_t^{z,z} = v_t(z)$ ,  $w_t^{z,\phi} = 1 - v_t(z)$ , and  $w_t^{z,z'} = 0$  if  $z \neq z'$ . For any  $z \in \bar{Z}_t$  and any  $\kappa \in \mathbb{I}_{t|t-1}$  or  $\kappa = z$ , the *external weight*  $w_{ex}^{\kappa,z}$  (scalar) is the weight corresponding to the association of the observations in  $Z_t \setminus \{z\}$  with false alarms, any of the remaining undetected individuals, or any remaining hypotheses in  $\mathbb{I}_{t|t-1} \setminus \{\kappa\}$  i.e.  $w_{ex}^{\kappa,z} \in [0, 1]$ , the multi-target marginal likelihood, can be seen as the assessment of the compatibility between the predicted laws  $(\{p_{t|t-1}^i\}_{i \in \mathbb{I}_{t|t-1}})$  and the collection of observations at the current time excluding the target with index  $\kappa$  and the observation  $z$ . This scalar can be expressed as

$$w_{ex}^{\kappa,z} = C'_t(\kappa, z) \prod_{\kappa' \in \mathbb{I}_{t|t-1} \setminus \{\kappa\}} \left[ w_t^{\kappa',\phi} + \sum_{z' \in Z_t \setminus \{z\}} \frac{w_t^{\kappa',z'}}{C_t(z')} \right] \quad (17)$$

where  $C_t(z) = w_t^{u,z}/w_t^{u,\phi} + v_t(z)/(1 - v_t(z))$  and where

$$C'_t(\kappa, z) = \frac{[w_t^{u,\phi}]^{n_{t|t-1}^u - \mathbf{1}_u(\kappa)}}{\left[ \prod_{z' \in Z_t \setminus Z'} (1 - v_t(z')) \right] \left[ \prod_{z' \in Z_t \setminus \{z\}} C_t(z') \right]} \quad (18)$$

with  $Z' = \emptyset$  when  $\kappa \in \mathbb{I}_{t|t-1}$  and  $Z' = \{z\}$  when  $\kappa$  corresponds to a false alarm ( $\kappa = z$ ). The hypotheses corresponding to false alarms are not indexed in the set  $\mathbb{I}_t$  since they are not considered for the next time step. Though they are ignored for the purpose of filtering, they need to be stored as they will be useful for track extraction (see section III-D).

The approximated multi-target configuration  $\mathcal{P}_t$  after the data update at time  $t$  is then given by  $\mathcal{P}_t = \{p_t^i, w_t^i, n_t^i\}_{i \in \mathbb{I}_t}$  where  $n_t^i = n_{t|t-1}^u$  if  $\mathbf{i} = u$  and  $n_t^i = 1$  otherwise. It

can also be stated that the collection of marginalized single-target laws  $\{p_t^i\}_{i \in \mathbb{I}_t}$  can be seen as single-target filters in interaction, where the weights of the filters are  $\{w_t^i\}_{i \in \mathbb{I}_t}$ . There are two assumptions that lead to the structure of the posterior weights (16), (17) of the hypotheses. The first one is for any  $\kappa, \kappa' \in \mathbb{I}_{t|t-1}$  such that  $\kappa \neq \kappa'$  and any  $z \in Z_t$ , it holds that  $\tilde{w}_t^{\kappa,z} \tilde{w}_t^{\kappa',z} \approx 0$ . This implies that the data association is moderately ambiguous i.e. it is related to sparsity of the scenario; the HISP filter is based on the sparsity assumption. The second assumption is that hypotheses are independent of each other. Particularly, the computation of the weight  $w_{ex}^{\kappa,z}$  does not involve combinatorial operations on the subsets of observations and/or hypotheses making the observation update step have a linear complexity with respect to the number of hypotheses and the number of observations i.e.  $\mathcal{O}(|\mathbb{I}_{t|t-1}| |Z_t|)$ . Thus, a complexity of the HISP filter complete recursion is  $\mathcal{O}(|\mathbb{I}_{t|t-1}| |Z_t|)$  since the computation of the terms  $w_{ex}^{\kappa,z}$  is the only part of it with a higher complexity.

### C. Pruning and Merging

Although the HISP filter has a linear complexity in the number of hypotheses and in the number of observations, reducing the computational cost by limiting the number of propagated hypotheses without a reasonable information loss is crucial while ensuring a meaningful track extraction. From the output of the HISP filter at time  $t$  with a multi-target configuration  $\mathcal{P}_t = \{p_t^i, w_t^i, n_t^i\}_{i \in \mathbb{I}_t}$ , the pruning and merging steps are given as follows:

- 1) A hypothesis  $i \in \mathbb{I}_t$  may have a negligible weight  $w_t^i$ . Such hypothesis can be pruned by retaining the subset of hypotheses having a weight greater than a threshold of  $\tau_p$ .
- 2) Some hypotheses  $I \subseteq \mathbb{I}_t$  may have probability densities  $p_t^i, i \in I$ , that are very close to each other. Such probability densities can be merged since they represent very similar information. Thus, the Mahalanobis distance between the given probability distributions with less than a threshold of  $\tau_m$  is used as a merging metric.
- 3) Some hypotheses  $I \subseteq \mathbb{I}_t$  may have the same observation path over the extraction window  $T$  so that they can be assumed to represent the same potential target. Such hypotheses can be merged into a single hypothesis with  $w = \sum_{i \in I} w_t^i$  if  $w \leq 1$  since hypotheses cannot have a weight strictly greater than 1.

After the pruning and merging steps, the multi-target configuration will be  $\tilde{\mathcal{P}}_t = \{\tilde{p}_t^i, \tilde{w}_t^i, \tilde{n}_t^i\}_{i \in \tilde{\mathbb{I}}_t}$ , and is used in the next time step.

### D. Track Extraction

Tracks, the subset of hypotheses that is the likeliest candidate to represent the population of targets in the scene, are extracted as follows from the multi-target configuration propagated by the HISP filter. The track extraction process has no effect on the filtering process and thus the set of hypotheses is not modified; it is merely for output. The simplest and efficient track extraction method is to select

the subset of hypotheses with the highest possible weights and whose observation paths agree with the observations collected during some sliding time window  $T$ . The posterior probabilities for each observation produced during this time window to be false alarms need to be computed and stored as hypotheses along with hypotheses corresponding to targets that disappeared during the time window. This is important to know all the observations collected in this time window for the purpose of track extraction. Given the temporary set of hypotheses  $\hat{\mathbb{I}}_t$  resulting from these modifications, the track extraction can be solved through the following optimization problem

$$\operatorname{argmax}_{I \subseteq \hat{\mathbb{I}}_t} \prod_{i \in I} \tilde{w}_t^i \quad (19)$$

subject to 1) the union of all observation paths over the time window  $T \subseteq \mathbb{T} \cap [0, t]$  must contain all the observations over this window, and 2) the observation paths in  $I$  must be pairwise compatible i.e. each observation cannot be used more than once. The solution to this problem is the same as the one for

$$\operatorname{argmax}_{I \subseteq \hat{\mathbb{I}}_t} \sum_{i \in I} \log \tilde{w}_t^i \quad (20)$$

with the same constraints since all  $\tilde{w}_t^i$  are strictly positive. Taking this way helps us to solve it using integer programming, for instance, using the GNU Linear Programming Kit (GLPK). The tracks that have been observed at least once in the sliding window are selected through this optimization problem. This track extraction approach is only one among many possible. It is one of the simplest that uses the structure of the filter instead of selecting hypotheses individually based on their weight, for example.

In video tracking context, specially when targets density is very high, two or more nearby targets can be detected as a single bounding box due to their extended nature. When these targets start to move apart, they might be detected by their own bounding boxes. This situation is similar to spawning of targets from the original target. However, spawning targets are currently not modelled in the HISP filter. Therefore, when tracks are extracted according to the above procedure, there are cases when the spawning targets take the same label as the original target. These cause difficulty to identify them as they share the same label. In this work, we use the weight propagated with each track (confirmed hypothesis) to discriminate them with the assumption that the original target has a maximum weight, after track extraction process. Thus, if two or more tracks with the same label are confirmed at the same time, we give new label(s) to those spawned target(s) except the original target with the assumption that the original target has a maximum weight and needs to retain the original label i.e. the spawned targets are treated as new births. This approach solves the problem of having the same label, however, it is rarely prone to identity switches since the spawned target(s) can have weight(s) greater than the original target violating our assumption. Note that this process is merely for output purpose as it does not affect the filtering process.

#### IV. DISCRIMINATIVE DEEP APPEARANCE LEARNING

Visual appearance information is very crucial for tracking multiple targets as it provides rich information to disambiguate nearby targets where only spatio-temporal information can not handle. In this work, we learn deep appearance features of targets using deep CNN and incorporate into the likelihood function of the HISP filter. We adopt ResNet50 [17] as the backbone network of our Verification-Identification architecture to learn appearance information of targets from a large-scale training data set.

##### A. Appearance Feature Likelihood

The appearance feature likelihood function  $g_t(z_w|x)$  is given by

$$g_t(z_w|x) = \frac{\exp(C^w(\mathbf{z}_w^i, \mathbf{z}_w^j))}{\exp(C^w(\mathbf{z}_w^i, \mathbf{z}_w^j)) + \exp(-C^w(\mathbf{z}_w^i, \mathbf{z}_w^j))}, \quad (21)$$

where  $C^w(\mathbf{z}_w^i, \mathbf{z}_w^j)$  is the cosine distance between appearance feature vectors  $\mathbf{z}_w^i$  and  $\mathbf{z}_w^j$  which are extracted from the detected object regions determined by the detection vectors  $z_d^i$  and  $z_d^j$ , respectively, using the learned deep appearance model in section IV-B. As can be seen from Eq. (13),  $z_d^i$  corresponds to the predicted measurement vector  $Hx$  and  $z_d^j$  corresponds to the current detection vector  $z_d$ . The cosine distance  $C^w(\mathbf{z}_w^i, \mathbf{z}_w^j)$  between appearance feature vectors  $\mathbf{z}_w^i$  and  $\mathbf{z}_w^j$  is given using their dot product and magnitude (norm) as

$$C^w(\mathbf{z}_w^i, \mathbf{z}_w^j) = \frac{\mathbf{z}_w^i \cdot \mathbf{z}_w^j}{\|\mathbf{z}_w^i\| \|\mathbf{z}_w^j\|}, \quad (22)$$

Since this appearance feature likelihood is integrated with the detection vector likelihood in Eq. (11), it is used not only for data association but also for track updates.

##### B. Verification-Identification Network Based Appearance Learning

We use ResNet50 in our Verification-Identification Network (VerIdNet) which is illustrated in Fig. 3. This network is basically a convolutional Siamese network that combines the verification and identification losses i.e. it optimizes three objectives: two identification losses and one verification loss. Though this type of architecture has been used in face recognition community [32], ours is more similar to [19]. However, unlike the one in [19] which learns a re-identification appearance model on only one data set (Market1501 [33] with 751 identities), we trained this network on agglomeration of data sets (which has a total of 6,654 identities) with longer epochs to learn more robust discriminative appearance features of targets.

Basically, verification and identification models are the two well known types of CNN structures. The verification model determines whether a pair of images belong to the same person or not (binary classification) i.e. it is a similarity metric. However, it does not consider the relationship between the image pairs and the other images in the data set (all annotated

information is not considered). On other hand, identification model takes full advantages of all annotated labels and treats the task as a multi-class recognition problem to learn a discriminative CNN embedding<sup>1</sup>, however, it does not take into account the similarity between image pairs. The VerIdNet takes the advantages of the two models to learn more robust discriminative appearance features of targets.

As shown in Fig. 3, the VerIdNet uses two ResNet50 models pre-trained on ImageNet [34] by removing the final fully-connected (FC) layer, and with additional three Convolutional Layers, Square Layer and three losses. The Square Layer compares the high-level 4096-dimensional embeddings by subtracting and squaring element-wisely. Moreover, softmax and cross-entropy loss are used in this VerIdNet. Thus, given a pair of images, the VerIdNet simultaneously predicts the IDs of the two images and their similarity score.

**Data preparation:** We collect the training data from multiple sources. From all the training data set of MOT15 (TUD-Stadmitte, TUD-Campus, PETS09-S2L1, ETH-Bahnhof and ETH-Sunnyday) and MOT16/17 (5 sequences), we produce about 521 person identities. MOT16 and MOT17 have the same training data set though MOT17 is claimed to have more accurate ground truth and is used in our experiment. From TownCentre data set [35], we also produce about 213 identities. In addition to these tracking data sets, we also use publicly available person re-identification data sets such as Market1501 data set [33] (736 identities from 751 as we restrict the number of images per identity to at least 4.), CUHK03 data set [36] (1367 identities), LPW data set [37] (1974 identities), and MSMT data set [38] (1141 identities). Including the tracking data sets into these public re-identification data sets for training our network allows the network to learn the inter-frame variations which is useful for improving the tracking performance. From all these data sets, we produce about 6,654 identities for training our network. 10% of this training set (of each person identity if the number of images for that identity is greater than 9) is used for validation; no validation for small class.

We resize all the training images to  $256 \times 256$  and then subtract the mean image from all the images, which is computed from all the training images. During training, we randomly crop all the images to  $224 \times 224$  and then mirror horizontally. We use a random order of images by reshuffling the data set. The positive pairs are generated by randomly sampling image patches (cropped images) from the same person identities whereas the negative pairs are the image patches corresponding to different classes/identities. We set the ratio between the positive and negative pairs to 1:1 initially and then multiply it by a factor of 1.01 every epoch until it reaches 1:4, similar to the work in [19]. This is due to the limited number of positive pairs that may cause the network to over-fit.

**Training:** We train the VerIdNet using softmax, cross-entropy loss and mini-batch Stochastic Gradient Descent (SGD). The mini-batch size is set to 20. After computing

<sup>1</sup>An embedding is a relatively low-dimensional space into which you can translate high-dimensional vectors i.e. semantically similar inputs close together in the embedding space.

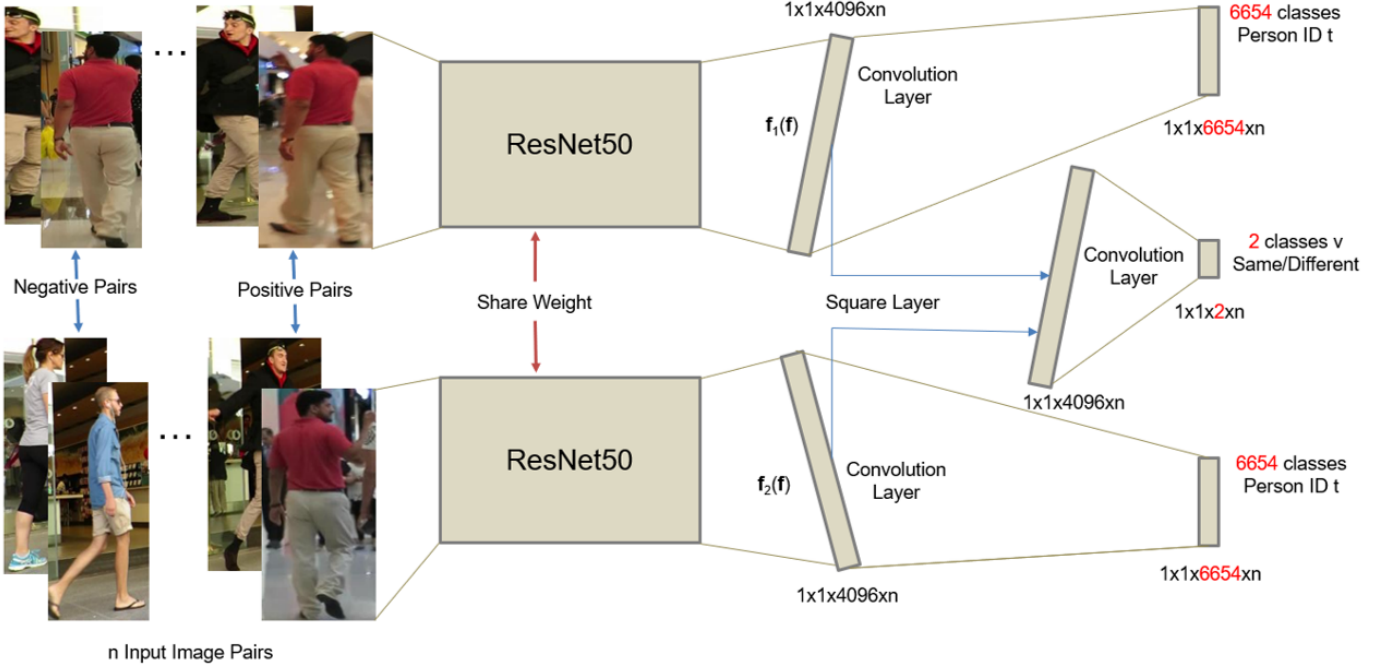


Fig. 3: Illustration of VerIdNet for discriminative deep appearance learning using two ResNet50 models.

all the gradients produced by every objective (there are three objectives in the VerIdNet), we add the weighted gradients together (1.0 for verification loss and 0.5 for the two identification losses) to update the network. We trained our model on a NVIDIA GeForce GTX 1050 GPU for 200 epochs (1 epoch is one sweep over all the training data), after which it generally converges, using MatConvNet [39]. We initialize the learning rate to  $10^{-4}$  for the first 75 epochs, to  $10^{-5}$  for the next 75 epochs and to  $10^{-6}$  for the last 50 epochs. In addition, we augment the training samples by random flipping horizontally as well as randomly shifting the cropping positions by no more than  $\pm 0.2$  of detection box of width or height for  $x$  and  $y$  dimensions, respectively, to increase more variation and thus reduce possible over-fitting. We use a dropout of 0.9 (setting the output of each hidden neuron to zero with probability 0.9) before the final convolution layer for reducing a possible over-fitting.

**Testing:** Two video sequences of MOT16/17 training data set (02 and 09) are used for testing of the VerIdNet. For this testing set, we produce about 66 person identities. As shown in Fig. 3, the two ResNet50 models share weights, therefore, we extract features by activating only one fine-tuned ResNet50 model. Thus, we get a 4,096-dimensional descriptor  $\mathbf{f}$  given a  $224 \times 224$  input image by feeding it forward to the ResNet50 in our network. Then, a cosine distance is computed between the extracted appearance feature vectors as in section IV-A. For evaluating the trained VerIdNet, we randomly sample about 800 positive pairs (the same identities) and 3200 negative pairs (different identities) from ground truth of MOT16/17-02 and MOT16/17-09 training data set (used as a testing set for our network). We use this larger ratio of negative pairs to mimic the positive/negative distribution during tracking. We use verification accuracy as an evaluation metric. Given a

pair of images, the cosine distance (using Eq. (22)) between their extracted deep appearance feature vectors using the learned model is computed. If the computed cosine-distance of positive pairs is greater than or equal to 0.75, they are assumed as correctly classified pairs. Similarly, if the computed cosine-distance of negative pairs is less than 0.75, they are assumed as correctly classified pairs. Accordingly, the VerIdNet trained on large-scale data sets (6,654 identities) gives about 98% accuracy while the work in [19] trained on only Market150 data set (751 identities) gives about 86% accuracy; our learned model gives a significant improvement.

## V. THE APPLICATIONS AND DETERMINATION OF THE VARIABLE VALUES IN THE HISP FILTER

The HISP filter can be implemented using any Bayesian filtering technique for each hypothesis, for instance, sequential Monte Carlo (SMC) [40] or Kalman filtering. In this work, we use the Kalman filter implementation of the HISP filter referred to as KF-HISP filter with the assumption of a linear Gaussian model. In this implementation scheme, a probability density, for instance  $p_t^i$ , is characterized by a multivariate normal distribution  $\mathcal{N}(m_t^i, P_t^i)$  where  $m_t^i$  is the mean and  $P_t^i$  is the covariance for  $i \in \mathbb{I}_t$ .

Our state vector includes the centroid positions, velocities, width and height of the bounding boxes, i.e.  $x_t = [p_{cx,xt}, p_{cy,xt}, \dot{p}_{x,xt}, \dot{p}_{y,xt}, w_{xt}, h_{xt}]^T$ . Similarly, the measurement is the noisy version of the target area in the image plane approximated with a  $w \times h$  rectangle centered at  $(p_{cx,xt}, p_{cy,xt})$  i.e.  $z_t = [p_{cx,zt}, p_{cy,zt}, w_{zt}, h_{zt}]^T$ .

A target state evolves from time  $t-1$  to time  $t$  through the Markov transition kernel  $q_t^\pi$  with matrices taking into account the box width and height at the given scale,

$$F_{t-1} = \begin{bmatrix} I_2 & \Delta I_2 & 0_2 \\ 0_2 & I_2 & 0_2 \\ 0_2 & 0_2 & I_2 \end{bmatrix},$$

$$Q_{t-1} = \sigma_v^2 \begin{bmatrix} \frac{\Delta^4}{4} I_2 & \frac{\Delta^3}{2} I_2 & 0_2 \\ \frac{\Delta^3}{2} I_2 & \Delta^2 I_2 & 0_2 \\ 0_2 & 0_2 & I_2 \end{bmatrix}, \quad (23)$$

where  $F$  and  $Q$  denote the state transition matrix and process noise covariance, respectively;  $I_n$  and  $0_n$  denote the  $n \times n$  identity and zero matrices, respectively, and  $\Delta = 1$  second is the sampling period defined by the time between consecutive frames.  $\sigma_v = 5$  pixels/ $s^2$  is the standard deviation of the process noise. The disappearance kernel  $q_t^\omega$  is assumed constant and verifies, for any  $x \in \mathbf{X}_t^\bullet$ ,  $q_t^\omega(\psi_{es}|x) = 10^{-2}$  (i.e. the probability of survival  $p_t^\pi$  of the targets is 0.99). The HISP filter is sensitive to  $p^\pi$ :  $p^\pi = 1$  implies that if an hypothesis is present almost surely then it will be displayed at all following time steps, alternatively, if  $p_t^\pi \leq p_d$  then hypotheses stop to be considered as tracks as soon as a detection failure happens. Thus, it is preferable to set the value of  $p^\pi$  greater than the value of the probability of detection  $p_d$  to handle some miss-detections.

Similarly, the measurement follows the observation model, Eq. (10), with matrices taking into account the box width and height,

$$H_t = \begin{bmatrix} I_2 & 0_2 & 0_2 \\ 0_2 & 0_2 & I_2 \end{bmatrix},$$

$$R_t = \sigma_r^2 \begin{bmatrix} I_2 & 0_2 \\ 0_2 & I_2 \end{bmatrix}, \quad (24)$$

where  $H_t$  and  $R_t$  denote the observation matrix and the observation noise covariance, respectively, and  $\sigma_r = 6$  pixels is the measurement standard deviation. The probability of detection is assumed to be constant across the state space and through time and is set to a value of  $p_d = 0.90$ . The false positives are independently and identically distributed (i.i.d), and the number of false positives per frame is Poisson-distributed with mean 10 (false alarm rate of  $v_t(z) \approx 4.8 \times 10^{-6}$ ; dividing the mean 10 by frame resolution).

The average number of appearing targets per frame  $n_t^\alpha$  is set to 0.1. This number is then divided uniformly across frame resolution to give the probability  $w_t^\alpha$  that any potential observation represents an appearing target. The distribution  $p_t^\alpha$  is uninformative since nothing is known about the appearing targets before the first observation. The distribution after the observation is determined by the current measurement and zero initial velocity used as a mean of the Gaussian distribution and using a predetermined initial covariance given in Eq. (25) for birth of targets.

$$P_t^\alpha = \text{diag}([100, 100, 25, 25, 20, 20]). \quad (25)$$

To reduce the computational cost, the pruning threshold  $\tau_p$  is set to  $10^{-3}$  and the merging threshold  $\tau_m$  is set to 4 pixels, and are used on the collection of individual posterior laws (probability densities). For track extraction, the sliding

time window  $T$  is set to 5. We set the maximum number of hypotheses to  $10^7$ .

## VI. EXPERIMENTAL RESULTS

To evaluate the performance of our proposed online tracker, HISP-DAL, we conduct extensive experiments on the MOT16 and MOT17 benchmark data sets [41], which are filmed on unconstrained environments and are widely used data sets for multiple people tracking. Thus, we compare the HISP-DAL against state-of-the-art online and offline tracking methods such as GM-PHD-HDA [2], DP-NMS [6], SMOT [42], CEM [5], JPDA-m [43], EAMTT [1], GMPHD-KCF [44], GM-PHD [45], GM-PHD-NIT [26], GM-PHD-DAL [3], HISP-T [21], JCmin-MOT [46], SAS-MOT17 [47], FPSN [48], OTCD-1 [49] and SORT17 [50]. We use the *public detections* provided by the MOT benchmark with a non-maximum suppression (NMS) of 0.3 for DPM detector (for both MOT16 and MOT17) and 0.5 for FRCNN and SDP detectors (for MOT17). We use the following evaluation metrics:

- **Multiple Object Tracking Accuracy (MOTA):** A summary of overall tracking accuracy in terms of false positives, false negatives and identity switches, which gives a measure of the tracker's performance at detecting objects as well as keeping track of their trajectories.
- **Multiple Object Tracking Precision [51] (MOTP):** A summary of overall tracking precision in terms of bounding box overlap between ground-truth and tracked location, which shows the ability of the tracker to estimate precise object positions.
- **Identification F1 (IDF1) score [52]:** The ratio of correctly identified detections (correctly labeled tracks) over the average number of ground-truth and computed detections (tracks).
- **Mostly Tracked targets (MT):** Percentage of mostly tracked targets (a target is tracked for at least 80% of its life span regardless of maintaining its identity) to the total number of ground truth trajectories.
- **Mostly Lost targets (ML) [53]:** Percentage of mostly lost targets (a target is tracked for less than 20% of its life span) to the total number of ground truth trajectories.
- **False Positives (FP):** Number of false detections.
- **False Negatives (FN):** Number of miss-detections.
- **Identity Switches (IDS<sub>w</sub>):** Number of times the given identity of a ground-truth track changes.
- **Fragmented trajectories (Frag):** Number of times a track is interrupted (compared to ground truth trajectory) due to miss-detection.

True positives are detections which have at least 50% overlap with their corresponding ground truth bounding boxes. For more detailed description of each metric, please refer to [41].

Quantitative evaluation of our proposed method with other trackers is compared in Table I on MOT16 benchmark data set. The Table shows that HISP-DAL outperforms both online and offline trackers listed in the table in terms of MOTA. Our tracker is also ranked 2nd in terms MT. In terms of MOTP, our tracker outperforms many online and offline trackers such as

CEM, SMOT, GM-PHD-HDA, HISP-T and JCmin-MOT. The number of ML and FN percentage is overall lower than many of the online and offline trackers such as CEM, DP-NMS, JPDP-m, GM-PHD-HDA, GM-PHD-N1T, GM-PG-DAL and JCmin-MOT. Similarly, IDF1 of our tracker is higher than many of the online and offline trackers; the number of IDSw and Frag is also lower than many of the online and offline trackers in the table. Our tracker also gives promising results on MOT17 benchmark data set as is quantitatively shown in Table II. It outperforms all other trackers in the table in MOTA. In terms of ML and FN, our tracker is ranked 2nd. Our tracker outperforms many of the online and offline trackers in terms of both MOTP and IDF1 as well. Similarly, the number of FP, IDSw and Frag is also lower than many of the trackers in the table.

The incorporation of deep appearance information improves the tracking performance as shown in Table I. Our proposed tracker, HISP-DAL, which uses the deep appearance features in addition to the spatio-temporal (motion) information outperforms the HISP-T tracker which uses only the motion information in terms of many metrics such as MOTA, IDF1, MOTP, IDSw and Frag. For instance, our proposed tracker increases MOTA and IDF1 values from 35.9 and 28.9 to 37.4 and 30.5, respectively. Thus, the construction of an augmented likelihood in a principled manner using the deeply learned CNN appearance features and motion information improves the tracking performance in terms of many evaluation metrics.

Examples of tracking results of all MOT17 test sequences using SDP detector except MOT17-07-SDP are shown in Figure 4; from left to right: MOT17-01-SDP, MOT17-03-SDP (top row), MOT17-06-SDP, MOT17-08-SDP (middle row), and MOT17-12-SDP, MOT17-14-SDP (bottom row). Three frames from MOT17-07-SDP are also shown in Figure 5. In all figures, the bounding boxes represent the tracking results with their color-coded identities. The MOT17-07-SDP shown in Figure 5 contains 54 tracks recorded by a moving camera in a sequence of 500 frames. Tracking in this sequence is a very challenging task, not only because the density of pedestrians is quite high, but also because significant camera motion makes the person trajectories to be both rough and discontinuous. Our tracker reasonably performs even on this sequence only with very few identity switches due to significant camera motion and detection failures.

Our proposed tracking algorithm is implemented in Matlab (not well optimized) on a i7 2.80 GHz core processor with 8 GB RAM. We use the MatConvNet [39] for CNN feature extraction where its forward propagation computation is transferred to a NVIDIA GeForce GTX 1050 GPU, and our tracker runs at about 3.3 frames per second (fps). The forward propagation for feature extraction and the track extraction steps are the two computationally expensive parts of our tracking algorithm.

## VII. CONCLUSIONS

We have developed a novel multi-target visual tracker based on the recently developed Hypothesized and Independent Stochastic Population (HISP) filter. We apply this filter for

tracking multiple targets in video sequences acquired under varying environmental conditions and targets density. We followed a tracking-by-detection approach using the public detections provided in the Multiple Object Tracking 2016 (MOT16) and MOT17 benchmark data sets. We also include a principled combination of motion and appearance information obtained from point detections and deep CNN features, respectively, into a single augmented likelihood for better tracking performance. Furthermore, we overcome the problem of identical labels that two or more nearby targets share through the employed track extraction approach by using the weight of the confirmed tracks which is very crucial in the case of video tracking. Results show that our method outperforms state-of-the-art trackers developed using both online and offline approaches on the MOT16 and MOT17 benchmark data sets in terms of tracking accuracy. This proposed online tracking algorithm can also be devised as a batch-based tracking algorithm using the track extraction method on all the video sequences rather than using a sliding window for better performance with its limitation for real-time applications. Using other optimization algorithms such as Lagrangian relaxation for the track extraction may also improve the performance. Making some changes to the network architecture such as replacing the softmax and cross entropy loss by the arcface [54] and focal loss [55], respectively, may improve the discriminative learning of appearance features of targets, which we may look into in our future work.

## REFERENCES

- [1] R. Sanchez-Matilla, F. Poiesi, and A. Cavallaro, "Online multi-target tracking with strong and weak detections," in *Computer Vision - ECCV 2016 Workshops - Amsterdam, The Netherlands, October 8-10 and 15-16, 2016, Proceedings, Part II*, 2016, pp. 84–99.
- [2] Y. Song and M. Jeon, "Online multiple object tracking with the hierarchically adopted GM-PHD filter using motion and appearance," in *IEEE/IEE The International Conference on Consumer Electronics (ICCE) Asia*, 2016.
- [3] N. L. Baisa, "Online multi-object visual tracking using a GM-PHD filter with deep appearance learning," in *2019 22nd International Conference on Information Fusion (FUSION)*, July 2019.
- [4] L. Leal-Taix, C. Canton-Ferrer, and K. Schindler, "Learning by tracking: Siamese CNN for robust target association," *IEEE Conference on Computer Vision and Pattern Recognition Workshops (CVPR), DeepVision: Deep Learning for Computer Vision.*, 2016.
- [5] A. Milan, S. Roth, and K. Schindler, "Continuous energy minimization for multitarget tracking," *IEEE Transactions on Pattern Analysis and Machine Intelligence*, vol. 36, no. 1, pp. 58–72, Jan 2014.
- [6] H. Pirsiavash, D. Ramanan, and C. C. Fowlkes, "Globally-optimal greedy algorithms for tracking a variable number of objects," in *CVPR 2011*, June 2011, pp. 1201–1208.
- [7] W. Luo, X. Zhao, and T. Kim, "Multiple object tracking: A literature review," *CoRR*, vol. abs/1409.7618, 2014. [Online]. Available: <http://arxiv.org/abs/1409.7618>
- [8] B.-N. Vo, M. Mallick, Y. Bar-Shalom, S. Coraluppi, R. O. III, R. Mahler, and B.-T. Vo, "Multitarget Tracking". Wiley Encyclopedia of Electrical and Electronics Engineering, Wiley, September 2015.
- [9] Y. Bar-Shalom, P. Willett, and X. Tian, *Tracking and Data Fusion: A Handbook of Algorithms*. YBS Publishing, 2011. [Online]. Available: <https://books.google.co.uk/books?id=2aOiuAAACAAJ>
- [10] C. Kim, F. Li, A. Ciptadi, and J. M. Rehg, "Multiple hypothesis tracking revisited," in *2015 IEEE International Conference on Computer Vision (ICCV)*, Dec 2015, pp. 4696–4704.
- [11] R. P. Mahler, *Advances in statistical multisource-multitarget information fusion*. Norwood: Artech House, 2014. [Online]. Available: <http://cds.cern.ch/record/2158275>



Tracker	Tracking Mode	MOTA $\uparrow$	MOTP $\uparrow$	IDF1 $\uparrow$	MT (%) $\uparrow$	ML (%) $\downarrow$	FP $\downarrow$	FN $\downarrow$	IDS $\downarrow$	Frag $\downarrow$
CEM [5]	offline	33.2	75.8	N/A	<b>7.8</b>	54.4	6,837	114,322	642	<b>731</b>
DP-NMS [6]	offline	32.2	76.4	31.2	5.4	62.1	<b>1,123</b>	121,579	972	944
SMOT [42]	offline	29.7	75.2	N/A	5.3	<b>47.7</b>	17,426	<b>107,552</b>	3,108	4,483
JPDF-m [43]	offline	26.2	76.3	N/A	4.1	67.5	3,689	130,549	<b>365</b>	<b>638</b>
GM-PHD-HDA [2]	online	30.5	75.4	<b>33.4</b>	4.6	59.7	5,169	120,970	<b>539</b>	<b>731</b>
GM-PHD-NIT [26]	online	33.3	<b>76.8</b>	25.5	5.5	56.0	<b>1,750</b>	116,452	3,499	3,594
GM-PHD-DAL [3]	online	35.1	<b>76.6</b>	26.6	7.0	51.4	2,350	111,886	4,047	5,338
HISP-T [21]	online	35.9	76.1	28.9	<b>7.8</b>	<b>50.1</b>	6,406	<b>107,905</b>	2,592	2,299
JCmin-MOT [46]	online	<b>36.7</b>	75.9	<b>36.2</b>	7.5	54.4	2,936	111,890	667	831
<b>HISP-DAL (ours)</b>	online	<b>37.4</b>	76.3	30.5	<b>7.6</b>	50.9	3,222	108,865	2,101	2,151

TABLE I: Tracking performance of representative trackers developed using both online and offline methods. All trackers are evaluated on the test data set of the **MOT16** [41] benchmark using public detections. The first and second highest values are highlighted by **red** and **blue**, respectively. Evaluation measures with ( $\uparrow$ ) show that higher is better, and with ( $\downarrow$ ) denote lower is better. N/A shows not available.

Tracker	Tracking Mode	MOTA $\uparrow$	MOTP $\uparrow$	IDF1 $\uparrow$	MT (%) $\uparrow$	ML (%) $\downarrow$	FP $\downarrow$	FN $\downarrow$	IDS $\downarrow$	Frag $\downarrow$
SAS-MOT17 [47]	offline	44.2	76.4	<b>57.2</b>	<b>16.1</b>	44.3	29,473	283,611	<b>1,529</b>	<b>2,644</b>
DP-NMS [6]	offline	43.7	76.9	N/A	12.6	46.5	<b>10,048</b>	302,728	4,942	5,342
FPSN [48]	online	<b>44.9</b>	76.6	<b>48.4</b>	<b>16.5</b>	<b>35.8</b>	33,757	<b>269,952</b>	7,136	14,491
EAMTT [1]	online	42.6	76.0	41.8	12.7	42.7	30,711	288,474	4,488	5,720
GM-PHD-KCF [44]	online	40.3	75.4	36.6	8.6	43.1	47,056	283,923	5,734	7,576
GM-PHD [45]	online	36.2	76.1	33.9	4.2	56.6	23,682	328,526	8,025	11,972
GM-PHD-DAL [3]	online	44.4	77.4	36.2	14.9	39.4	19,170	283,380	11,137	13,900
OTCD-1 [49]	online	<b>44.9</b>	77.4	42.3	14.0	44.2	<b>16,280</b>	291,136	<b>3,573</b>	5,444
GM-PHD-NITr [26]	online	42.1	<b>77.7</b>	33.9	11.9	42.7	18,214	297,646	10,698	10,864
SORT17 [50]	online	43.1	<b>77.8</b>	39.8	12.5	42.3	28,398	287,582	4,852	7,127
GM-PHD-SHA [2]	online	43.7	76.5	39.2	11.7	43.0	25,935	287,758	3,838	<b>5,056</b>
<b>HISP-DAL (ours)</b>	online	<b>45.4</b>	77.3	39.9	14.8	<b>39.2</b>	21,820	<b>277,473</b>	8,727	7,147

TABLE II: Tracking performance of representative trackers developed using both online and offline methods. All trackers are evaluated on the test data set of the **MOT17** benchmark using public detections. The first and second highest values are highlighted by **red** and **blue**, respectively. Evaluation measures with ( $\uparrow$ ) show that higher is better, and with ( $\downarrow$ ) denote lower is better. N/A shows not available.

- [12] —, “Multitarget bayes filtering via first-order multitarget moments,” *IEEE Trans. on Aerospace and Electronic Systems*, vol. 39, no. 4, pp. 1152–1178, 2003.
- [13] J. Houssineau and D. E. Clark, “Multitarget filtering with linearized complexity,” *IEEE Transactions on Signal Processing*, vol. 66, no. 18, pp. 4957–4970, Sep. 2018.
- [14] E. Delande, J. Houssineau, J. Franco, C. Frh, and D. Clark, “A new multi-target tracking algorithm for a large number of orbiting objects,” *27th AAS/AIAA Space Flight Mechanics Meeting*, 2017.
- [15] E. Delande, J. Houssineau, J. Franco, C. Frueh, D. Clark, and M. Jah, “A new multi-target tracking algorithm for a large number of orbiting objects,” *Advances in Space Research*, vol. 64, no. 3, pp. 645 – 667, 2019. [Online]. Available: <http://www.sciencedirect.com/science/article/pii/S0273117719302728>
- [16] A. Krizhevsky, I. Sutskever, and G. E. Hinton, “ImageNet classification with deep convolutional neural networks,” in *Advances in Neural Information Processing Systems 25*, F. Pereira, C. Burges, L. Bottou, and K. Weinberger, Eds., 2012, pp. 1097–1105.
- [17] K. He, X. Zhang, S. Ren, and J. Sun, “Deep residual learning for image recognition,” *CoRR*, vol. abs/1512.03385, 2015.
- [18] S. Ren, K. He, R. B. Girshick, and J. Sun, “Faster R-CNN: towards real-time object detection with region proposal networks,” *CoRR*, vol. abs/1506.01497, 2015. [Online]. Available: <http://arxiv.org/abs/1506.01497>
- [19] Z. Zheng, L. Zheng, and Y. Yang, “A discriminatively learned CNN embedding for person re-identification,” *CoRR*, vol. abs/1611.05666, 2016.
- [20] A. Sadeghian, A. Alahi, and S. Savarese, “Tracking the untrackable: Learning to track multiple cues with long-term dependencies,” *CoRR*, vol. abs/1701.01909, 2017. [Online]. Available: <http://arxiv.org/abs/1701.01909>
- [21] N. L. Baisa, “Online multi-target visual tracking using a HISP filter,” in *Proceedings of the 13th International Joint Conference on Computer Vision, Imaging and Computer Graphics Theory and Applications - Volume 5: VISAPP, INSTICC*. SciTePress, 2018, pp. 429–438.
- [22] B.-N. Vo and W.-K. Ma, “The Gaussian mixture probability hypothesis density filter,” *Signal Processing, IEEE Transactions on*, vol. 54, no. 11, pp. 4091–4104, Nov 2006.
- [23] N. L. Baisa, D. Bhowmik, and A. Wallace, “Long-term correlation tracking using multi-layer hybrid features in sparse and dense environments,” *Journal of Visual Communication and Image Representation*, vol. 55, pp. 464 – 476, 2018. [Online]. Available: <http://www.sciencedirect.com/science/article/pii/S1047320318301536>
- [24] N. L. Baisa, “Single to multiple target, multiple type visual tracking,” Ph.D. dissertation, Heriot-Watt University, 06 2018.
- [25] N. L. Baisa and A. Wallace, “Multiple target, multiple type filtering in the RFS framework,” *Digital Signal Processing*, vol. 89, pp. 49 – 59, 2019. [Online]. Available: <http://www.sciencedirect.com/science/article/pii/S1051200418303166>
- [26] —, “Development of a N-type GM-PHD filter for multiple target, multiple type visual tracking,” *Journal of Visual Communication and Image Representation*, vol. 59, pp. 257 – 271, 2019. [Online]. Available: <http://www.sciencedirect.com/science/article/pii/S1047320319300343>
- [27] B. Vo, B. Vo, and D. Phung, “Labeled random finite sets and the bayes multi-target tracking filter,” *IEEE Transactions on Signal Processing*, vol. 62, no. 24, pp. 6554–6567, Dec 2014.
- [28] B. Vo, B. Vo, and H. G. Hoang, “An efficient implementation of the generalized labeled multi-bernoulli filter,” *IEEE Transactions on Signal Processing*, vol. 65, no. 8, pp. 1975–1987, April 2017.
- [29] D. Y. Kim, “Online multi-object tracking via labeled random finite set with appearance learning,” in *2017 International Conference on Control, Automation and Information Sciences (ICCAIS)*, Oct 2017, pp. 181–186.
- [30] E. Delande, J. Houssineau, and D. Clark, “Multi-object filtering with stochastic populations,” *arXiv*, vol. 1501.04671v2, 2016. [Online]. Available: <https://arxiv.org/abs/1501.04671v2>
- [31] Z. Fu, F. Angelini, S. M. Naqvi, and J. A. Chambers, “GM-PHD filter based online multiple human tracking using deep discriminative correlation matching,” in *2018 IEEE International Conference on Acoustics, Speech and Signal Processing (ICASSP)*, April 2018, pp. 4299–4303.
- [32] Y. Sun, X. Wang, and X. Tang, “Deep learning face representation by joint identification-verification,” in *NIPS*, 2014.



Fig. 4: Sample results on several sequences of MOT17 data sets using SDP detector; bounding boxes represent the tracking results with their color-coded identities. From left to right: MOT17-01-SDP, MOT17-03-SDP (top row), MOT17-06-SDP, MOT17-08-SDP (middle row), and MOT17-12-SDP, MOT17-14-SDP (bottom row). The videos of tracking results are available on the MOT Challenge website <https://motchallenge.net/>.

- [33] L. Zheng, L. Shen, L. Tian, S. Wang, J. Wang, and Q. Tian, "Scalable person re-identification: A benchmark," in *2015 IEEE International Conference on Computer Vision (ICCV)*, Dec 2015, pp. 1116–1124.
- [34] O. Russakovsky, J. Deng, H. Su, J. Krause, S. Satheesh, S. Ma, Z. Huang, A. Karpathy, A. Khosla, M. Bernstein, A. C. Berg, and L. Fei-Fei, "ImageNet Large Scale Visual Recognition Challenge," *International Journal of Computer Vision (IJCV)*, vol. 115, no. 3, pp. 211–252, 2015.
- [35] B. Benfold and I. Reid, "Stable multi-target tracking in real-time surveillance video," in *CVPR*, June 2011, pp. 3457–3464.
- [36] W. Li, R. Zhao, T. Xiao, and X. Wang, "Deepreid: Deep filter pairing neural network for person re-identification," in *2014 IEEE Conference on Computer Vision and Pattern Recognition*, June 2014, pp. 152–159.
- [37] G. Song, B. Leng, Y. Liu, C. Hetang, and S. Cai, "Region-based quality estimation network for large-scale person re-identification," *CoRR*, vol. abs/1711.08766, 2017. [Online]. Available: <http://arxiv.org/abs/1711.08766>
- [38] L. Wei, S. Zhang, W. Gao, and Q. Tian, "Person transfer GAN to bridge domain gap for person re-identification," *CoRR*, vol. abs/1711.08565, 2017. [Online]. Available: <http://arxiv.org/abs/1711.08565>
- [39] A. Vedaldi and K. Lenc, "MatConvNet – convolutional neural networks for matlab," in *Proceedings of the 25th annual ACM international conference on Multimedia*, 2015.
- [40] J. Houssineau, D. E. Clark, and P. Del Moral, "A sequential monte carlo approximation of the HISP filter," in *Signal Processing Conference (EUSIPCO), 2015 23rd European*. IEEE, 2015, pp. 1251–1255.
- [41] A. Milan, L. Leal-Taixé, I. Reid, S. Roth, and K. Schindler, "MOT16: A benchmark for multi-object tracking," *arXiv:1603.00831 [cs]*, Mar. 2016, arXiv: 1603.00831. [Online]. Available: <http://arxiv.org/abs/1603.00831>
- [42] C. Dicle, O. I. Camps, and M. Szaier, "The way they move: Tracking multiple targets with similar appearance," in *2013 IEEE International Conference on Computer Vision*, Dec 2013, pp. 2304–2311.
- [43] S. H. Rezatofighi, A. Milan, Z. Zhang, Q. Shi, A. Dick, and I. Reid, "Joint probabilistic data association revisited," in *2015 IEEE International Conference on Computer Vision (ICCV)*, Dec 2015, pp. 3047–3055.
- [44] T. Kutschbach, E. Bochinski, V. Eiselein, and T. Sikora, "Sequential





Fig. 5: Sample results on the sequence MOT17-07-SDP (using SDP detector); bounding boxes represent the tracking results with their color-coded identities, for frames 376, 386 and 395 from top to bottom. The video of tracking results are available on the MOT Challenge website <https://motchallenge.net/>.

- sensor fusion combining probability hypothesis density and kernelized correlation filters for multi-object tracking in video data,” in *2017 14th IEEE International Conference on Advanced Video and Signal Based Surveillance (AVSS)*, Aug 2017, pp. 1–5.
- [45] V. Eiselein, D. Arp, M. Ptzold, and T. Sikora, “Real-time multi-human tracking using a probability hypothesis density filter and multiple detectors,” in *2012 IEEE Ninth International Conference on Advanced Video and Signal-Based Surveillance*, Sep. 2012, pp. 325–330.
- [46] A. Boragule and M. Jeon, “Joint cost minimization for multi-object tracking,” in *2017 14th IEEE International Conference on Advanced Video and Signal Based Surveillance (AVSS)*, Aug 2017, pp. 1–6.
- [47] A. Maksai and P. Fua, “Eliminating exposure bias and metric mismatch in multiple object tracking,” in *The IEEE Conference on Computer Vision and Pattern Recognition (CVPR)*, June 2019.
- [48] S. Lee and E. Kim, “Multiple object tracking via feature pyramid siamese networks,” *IEEE Access*, vol. 7, pp. 8181–8194, 2019.
- [49] Q. Liu, B. Liu, Y. Wu, W. Li, and N. Yu, “Real-time online multi-object tracking in compressed domain,” *IEEE Access*, vol. 7, pp. 76 489–76 499, 2019.
- [50] A. Bewley, Z. Ge, L. Ott, F. Ramos, and B. Upcroft, “Simple online and realtime tracking,” in *2016 IEEE International Conference on Image Processing (ICIP)*, Sep. 2016, pp. 3464–3468.
- [51] R. Kasturi, D. Goldgof, P. Soundararajan, V. Manohar, J. Garofolo, R. Bowers, M. Boonstra, V. Korzhova, and J. Zhang, “Framework for performance evaluation of face, text, and vehicle detection and tracking in video: Data, metrics, and protocol,” *IEEE Transactions on Pattern Analysis and Machine Intelligence*, vol. 31, no. 2, pp. 319–336, Feb 2009.
- [52] E. Ristani, F. Solera, R. S. Zou, R. Cucchiara, and C. Tomasi, “Performance measures and a data set for multi-target, multi-camera tracking,” in *Computer Vision - ECCV 2016 Workshops - Amsterdam, The Netherlands, October 8-10 and 15-16, 2016, Proceedings, Part II*, 2016, pp. 17–35. [Online]. Available: [https://doi.org/10.1007/978-3-319-48881-3\\_2](https://doi.org/10.1007/978-3-319-48881-3_2)
- [53] Y. Li, C. Huang, and R. Nevatia, “Learning to associate: Hybridboosted multi-target tracker for crowded scene,” in *In CVPR*, 2009.
- [54] J. Deng, J. Guo, N. Xue, and S. Zafeiriou, “Arcface: Additive angular margin loss for deep face recognition,” in *The IEEE Conference on Computer Vision and Pattern Recognition (CVPR)*, June 2019.
- [55] T. Lin, P. Goyal, R. B. Girshick, K. He, and P. Dollár, “Focal loss for dense object detection,” *CoRR*, vol. abs/1708.02002, 2017. [Online]. Available: <http://arxiv.org/abs/1708.02002>